

1 **Turbulent heat transfer as a control of platelet ice growth in**
2 **~~supercool~~ supercooled under-ice ocean boundary-layers**

3

4 **M.G. McPhee¹, C.L. Stevens^{2,3}, I.J. Smith⁴ and N.J. Robinson²**

5 [1] McPhee Research Company, Naches Washington, USA.

6 [2] National Institute for Water and Atmospheric Research, Greta Point Wellington, New
7 Zealand.

8 [3] University of Auckland, Dept. Physics, New Zealand

9 [4] University of Otago, Dept. Physics, New Zealand.

10 Correspondence to: C.L. Stevens NIWA 301 Evans Bay Pde, Kilbirnie PO Box 14-901, 6021,
11 New Zealand (c.stevens@niwa.co.nz)

12

13

1 Abstract

2 Late winter measurements of turbulent quantities in tidally modulated flow under land-fast sea
3 ice near the Erebus Glacier Tongue, McMurdo Sound, Antarctica, identified processes that
4 influence growth at the interface of an ice surface in contact with ~~supercool~~supercooled
5 seawater. The data ~~suggest~~show that turbulent heat exchange at the ocean-ice boundary is
6 characterized by the product of friction velocity and (negative) water temperature departure
7 from freezing, analogous to similar results for moderate melting rates in seawater above
8 freezing. Platelet ice growth appears to increase the hydraulic roughness (drag) of fast ice
9 compared with undeformed fast ice without platelets. ~~We hypothesize that p~~Platelet growth in
10 ~~supercool~~supercooled water under thick ice ~~is~~appears to be rate-limited by turbulent heat
11 transfer and that this is a significant factor to be considered in mass transfer at the under-side
12 of ice shelves and sea ice in the vicinity of ice shelves.

13

14 1 Introduction

15 In addition to seaward advection, calving and basal melting, the distribution of mass in
16 ice shelves depends on the so-called ice pump (Lewis and Perkin, 1986). By this mechanism,
17 water warmer than the in situ freezing point temperature, typically High Salinity Shelf Water
18 entering the under-shelf cavity, encounters glacial ice at, ~~or near, high pressures, e.g., near the~~
19 ~~grounding line. The, where it is local~~ cooling and freshening by basal melting (BM, Figure
20 1) of the ice shelf underside all happens at high local pressure. The resultant buoyant water
21 circulates to lower pressure regions as the glacier base thins toward the terminus, and in the
22 process may become ~~supercool~~supercooled relative to its in situ pressure (Foldvik and Kvinge,
23 1974). Supercooled Ice Shelf Water (ISW) is formed. ~~Supercool~~Supercooled water can then
24 deposit ice by direct growth of ice crystals attached at the ice underside, or by upward migration

1 of frazil crystals suspended by turbulence in the water ([Dieckmann et al 1986](#)). In this way,
2 fresh glacial ice near the grounding line transforms to marine ice (Langhorne 2008). Evidence
3 from icebergs (Kipfstuhl et al., 1992), borehole (Craven, et al., 2005) and radar studies
4 (Engelhardt and Determann, 1987; Robin et al., 1983; Holland, et al., 2009) indicate that marine
5 ice can reach appreciable thicknesses, and that the ice pump is active under shelves where the
6 water entering the cavity is near freezing.

7 Formation of marine ice (~~(ML-Figure 1~~[Figure 1](#)) under ice shelves is difficult to observe
8 directly (Craven et al. 2015), but similar effects are readily observed beneath nearby sea ice
9 (e.g. Robinson et al., 2014; Hoppmann et al. 2015; Langhorne et al. 2015; Hughes et al. 2015).
10 For example in McMurdo Sound, Antarctica, sea ice crystals that have formed in
11 ~~superecools~~[supercooled](#) water have been observed and reported since the British National
12 Antarctic (Discovery) Expedition of 1901–04 (Hodgson, 1907) and the British Antarctic (Terra
13 Nova) Expedition of 1910-1913 (Wright and Priestley, 1922). Crystals observed in McMurdo
14 Sound have reported to be up to 250 mm in diameter (Robinson et al, 2014; Smith et al., 2001).
15 In part because of their size [and aspect ratio, and that turbulent suspension is not a direct driver,](#)
16 these crystals are ~~now known~~[identified](#) as “platelet ice”. They have been observed attached to
17 the underside of sea ice (Gow et al., 1998), often forming layers 2-3 m thick (Dayton et al.,
18 1969) and in some places as much as 8 m thick (Hughes et al. 2014). Platelet ice crystals have
19 been observed to become incorporated into the sea ice by subsequent congelation growth
20 (Jeffries et al., 1993).

21 The presence of ~~superecools~~[supercooled](#) water measured below sea ice (Lewis and
22 Perkin, 1985; Smith et al., 2001), and the abundance of platelet ice, has been linked to locations
23 of observed supercooling (Crocker and Wadhams, 1989) and to the ocean currents from beneath
24 the ice shelf (Leonard et al., 2011; Fer et al. 2012). Evidence of this link is provided by the

1 thicker accumulations of platelet ice (i.e. a sub-ice platelet layer ~~PL-Figure 1~~Figure 1) found on
2 the western side of McMurdo Sound (Dempsey et al., 2010; Hughes et al., 2014; Robinson et
3 al., 2014), compared to that ~~than~~ on the east (Gow et al., 1998; Jeffries et al., 1993, Dempsey
4 et al., 2010) where platelet ice only starts to form in late winter (Paige, 1966). Leonard et al.
5 (2006) and Mahoney et al. (2011) reported acoustic and video evidence that platelet ice crystals
6 begin as small crystals (2-20 mm) that become larger once attached to the sea ice cover above.

7 Based on heat and mass balance measurements within the ice column, the residual
8 oceanic heat flux associated with incorporated platelet ice has been reported as negative (i.e.,
9 heat moves downwards into the ocean) by several authors (Gough et al., 2012; Purdie et al.,
10 2006; Smith et al., 2012; 2015) with values of as large as -30 W m^{-2} or more reported elsewhere
11 (Purdie et al., 2006; Smith et al., 2001). Smith et al. (2001) noted that forced convection was
12 needed to account for the amount of platelet ice observed in McMurdo Sound, and Smith et al.
13 (2001) and Stevens et al. (2009) estimated kinematic eddy viscosities of $2 \times 10^{-5} \text{ m}^2 \text{ s}^{-1}$ and
14 $5 \times 10^{-4} \text{ m}^2 \text{ s}^{-1}$, respectively, in supercool water in McMurdo Sound. Smith et al. (2012) observed
15 episodic growth of individual platelet ice crystals, with periods of growth at least an order of
16 magnitude faster than the growth of the bulk sea ice. They suggested that variable currents were
17 responsible for the episodic nature of the crystal growth. The appearance of these supercooling-
18 induced crystals is not limited to the western margin of the Ross Ice Shelf, with observations
19 made in other cold-cavity systems sampled to date (Dieckmann et al. 1986; Craven et al. 2014;
20 Hoppmann et al. 2015; Langhorne et al. 2015).

21 The ~~presentis~~ work seeks to answer the questions (i) if and how the growth of platelet
22 ice at a ~~supercool~~ supercooled ice-ocean interface impacts the physical characteristics of the
23 interface, including hydraulic roughness and the rate of heat transfer in the water column, and
24 (ii) what feedbacks might exist. Direct turbulence measurements make this possible by

1 enabling characterisation of the boundary-layer and direct measurement of heat fluxes. This
2 facilitates improved parameterization of exchange processes in terms of mean quantities and
3 will enhance the modeling of the ice-pump deposition phase in ice shelf cavities (Gwyther et al
4 2015) as well as estimation of the spatial envelope of sea ice growth influenced by these cavities
5 (Langhorne et al. 2015).

6

7 **2 Methods**

8 **2.1 Field camp and instrumentation**

9 In October and November, 2010, the New Zealand National Institute Water and
10 Atmospheric Research (NIWA) established a temporary station (Erebus Field Camp -- EFC)
11 on fast (immobile) sea ice near Erebus Glacier Tongue (EGT) in McMurdo Sound, Antarctica.
12 The general layout of EFC and its location relative to nearby geographic features is described
13 by Stevens et al. (2014) (Figure 2). Included in the deployment was instrumentation designed
14 to accurately measure current, temperature, and salinity in tidal flow beneath the stationary sea
15 ice, at a resolution sufficiently small to enable turbulent fluxes of momentum, heat, and salt to
16 be quantified.

17 A top-mounted mooring was deployed in 350 m of water, 2.5 km to the SW of the EFC
18 at 77° 42.7730 S, 166° 21.4350 E, spanning the period in question. This mooring contained
19 three Aanderaa RCM-9 units coupled with SBE 37 Microcat temperature, salinity, and pressure
20 recorders (Seabird Electronics, USA). The current meter/Microcat pairs were located at depths
21 of 50, 150, and 300 m. Upon recovery of the mooring it was found that the line had lifted
22 sufficiently so that the top 10 m had frozen into the growing sub-ice platelet layer. This has
23 been encountered previously on instrument deployments when the buoyancy force from platelet

1 accretion on mooring lines had overwhelmed the mooring ballast. The remote nature of the
2 field camp meant it was not possible to deploy very heavy ballast blocks.

3 Flux measurements near the ice/ocean interface were made with turbulence instrument
4 clusters (TICs), each comprising an acoustic-Doppler velocimeter (Sontek ADVOcean, 5
5 MHz), mounted with its fixed sample volume in the same plane as a nearby Sea-Bird
6 Electronics temperature (SBE 3F)/conductivity (SBE 4) pair. Conductivity measurements
7 were supplemented by a dual electrode microstructure conductivity instrument (SBE 7). The
8 velocity sensors have a resolution of 0.1 cm s^{-1} and an accuracy of $\pm 1\%$ of measured velocity.
9 The dynamic range of the conductivity signal is typically large relative to instrument
10 sensitivity with an initial accuracy of $\pm 0.0003 \text{ S m}^{-1}$. The thermometers have an initial
11 accuracy of $\pm 0.001 \text{ }^\circ\text{C}$ and a stability $0.002 \text{ }^\circ\text{C}$ per year typically along with a self-heating
12 error $< 0.0001 \text{ }^\circ\text{C}$ in still water. Here we assume a working accuracy for the temperature
13 sensors of 5 mK. TICs configured as above have been deployed under ice during several
14 previous projects (McPhee, 2008a; MCPhee et al., 2008; MCPhee et al., 2013; Sirevaag et al.,
15 2010) and shown to measure well into the inertial subrange of the turbulent kinetic energy
16 spectrum, hence adequately capturing the covariance of vector and scalar variables in
17 turbulent flows.

18 The TICs were deployed on separate suspended masts ([Figure 2](#)) under fast sea
19 ice about 2.15 m in initial thickness. Mast A included two TICs mounted 1 and 3 m below the
20 ice on a fixed mast suspended through a 1 m diameter hole, located about 140 m from the edge
21 of EGT. Mast B, located closer (40 m) to the glacier tongue, included two TICs mounted 4 m
22 apart on a rigid mast that could be lowered by cable to depths up to 70 m.

23 **2.2 Turbulence analysis**

24 Time series of three velocity components, temperature, and salinity derived from

1 temperature and conductivity were segmented into 15-min realizations for calculating
2 turbulence statistics, including the rate of dissipation of turbulent kinetic energy ϵ , following
3 the method described by McPhee (2008a). Currents averaged over each realization were rotated
4 into a reference frame such that mean vertical and cross-stream horizontal components
5 vanished, from which the velocity perturbation components were resolved (u' , v' and w').
6 Linear trends were then removed, then “area-preserving” (weighted) spectra were calculated,
7 and transformed to the wave-number (spatial) domain under the frozen field hypothesis. Ice
8 nucleation on instruments immersed in ~~supercool~~-supercooled water significantly degraded
9 their performance after just a few tidal cycles. This can affect both ADVs and conductivity
10 sensors. We used the criteria identified in McPhee et al. (2013) to remove affected data. Ice
11 accreting on the ADV hydrophones increased noise at higher frequencies, eventually leading to
12 ~~nonsensical~~-incorrect velocities. Consequently, we placed added emphasis on ensuring that
13 turbulent spectra exhibited key elements including a peak in the area-preserving spectrum of
14 vertical velocity variance and a reasonable fall-off to the -2/3 slope in the log-log representation
15 of the area-preserving spectrum (McPhee, 1994; 2008a). Each 15 minute spectrum was
16 evaluated for a discernible peak in the area- preserving vertical velocity variance spectrum, and
17 if found to be viable, was included in a three-hour grouping of realizations to determine
18 mean statistics.

19 Friction speed, u_* , (the square root of kinematic Reynolds stress magnitude) was
20 estimated by averaging covariance statistics, i.e.,

$$21 \quad u_* = \left(\langle u'w' \rangle^2 + \langle v'w' \rangle^2 \right)^{1/4} \quad (1)$$

22 where we have invoked Taylor’s frozen field hypothesis linking measurements in the time
23 domain at a single location to ensemble statistics. After identifying the peak in each spectrum,
24 a high-order polynomial was fitted to wavenumbers in its vicinity, which was then analyzed to

Formatted: Font: Symbol

1 determine the wavenumber where the negative slope reached or exceeded 2/3, taken as
2 signifying spectral levels in the inertial subrange. The turbulent kinetic energy (TKE)
3 dissipation rate was estimated from [\(see e.g. Tennekes and Lumley, 1972\)](#)

$$\varepsilon^{2/3} = \frac{3}{4\alpha_\varepsilon} S_{ww}(k) k^{5/3} \quad (2)$$

4 where S_{ww} is the spectral density evaluated at angular wave number k , in the inertial subrange,
5 and α_ε is the Kolmogorov constant for the along-stream spectrum (0.51).

6 By assuming that flow within 1 m of the boundary lies within the so-called surface layer,
7 where stress is nearly constant and the velocity profile is logarithmic, then TKE production rate
8 by current shear is

$$P_s = \tau \frac{\partial u}{\partial z} = \frac{u_*^3}{\kappa |z|} \quad (3)$$

9 where κ is Kàrmàn's constant (0.4). [It is possible that buoyancy effects are also contributing](#)
10 [to the turbulence and this can be examined by comparing production and dissipation rates.](#)

11 **3 Results**

12 The present data come from [the "springs" period of the spring-neap tidal cycle](#) (Figure
13 3a) [in order to experience the widest range of flow speeds](#), although the tidal ~~flow effect~~ is only
14 weakly manifest in the far-field thermal structure (Figure 3b). No data were retrieved from this
15 [far-field](#) mooring at depths shallower than 50 m due to platelet growth effects. Indeed, as well
16 as the incorporation of the upper 10 m of the instrumented mooring line into the growing sea
17 ice, the mooring line itself was subject to ice accumulation-driven buoyancy-driven rise of 8 m
18 in a 50 day period although the lift was only around 1 m during the collection of the data in

1 (Figure 3). The 50 m data remain around -1.91 to -1.92 ° C.

2 ~~_____~~At the mast site, during the measurement period, ~~profiles made with the mobile TIC~~
3 ~~mast B indicated that the water column was isothermal to about 40 m. In addition data described~~
4 ~~in Stevens et al (2014) from the same campaign support the contention that, to within +/-5mK,~~
5 ~~the upper 40 m was isothermal. the water column was isothermal to about 40 m depth, with~~
6 ~~†The upper 15 m exhibited~~ temperatures below the pressure-dependent freezing temperature,
7 i.e., in-situ supercool, ~~down to about 15 m~~. The growth of ice on the far-field mooring was
8 corroborated by platelet growth on the cable suspending Mast B. At Mast A (TICs at 1 and 3 m
9 below the ice undersurface) ice accretion on the instruments limited the duration of acceptable
10 measurements to about two diurnal cycles (~60 h) ending early (UT) on DOY (day of year)
11 301. Shortly afterwards, Mast A was recovered, and thereafter Mast B was generally stationed
12 below the ~~supercool-supercooled~~ zone at depths ranging from 18 to 62 m, so as to minimize ice
13 accretion. Here we emphasize data from Mast A to address conditions near the horizontal fast
14 ice/ocean interface.

Formatted: Normal, Left, Line spacing: Double

15 ~~Spring tide~~ ~~Data~~ recorded during spring tides provide the largest velocity range and
16 also the largest horizontal advection of different water masses. Currents measured 1 m below
17 the ice/water boundary at Mast A from late on 25 Oct 2010 (DOY 298) to early on 28 Oct
18 (Figure 4a) show a significant tidal signal resulting in speeds up to around 0.15 m s⁻¹. This is
19 superimposed upon a steadier westward flow strong enough to prevent current reversal (Figure
20 4b) either through flow rectification or regional circulation (Stevens et al. 2014). This was
21 confirmed over a 10-day period beginning ~~with on DOY~~ ~~300~~, where currents measured in
22 the upper 60 m of the water column at the Mast B site ranged from 0.03 to 0.28 m s⁻¹ westward
23 (Stevens et al. 2014). Salinity shows a slowly increasing trend of around 0.0075 PSU/day that
24 is interrupted briefly ~~at slack water~~ during low flows (“slack water”) at high and low tide (Fig.

Formatted: Indent: First line: 1.27 cm

1 4c). In near-freezing waters, salinity dominates ~~influence on~~ buoyancy and so these
 2 perturbations are likely some form of propagating feature in the density structure. Certainly,
 3 the features in salinity at DOY 299.3-299.5 coincide with the directional change in Fig. 4b.
 4 Temperature measurements (Fig. 4d) on the other hand do not have obvious signatures
 5 connected to the flow. This is not uncommon at these temperatures where there is almost no
 6 thermal contribution to density. The record shows that water 1 m below the ice remained, on
 7 average, 8.7 mK below freezing. The salinity trend's influence on the freezing point is apparent
 8 in Figure 4d. This trend is largely mirrored in the measured temperature.

9 Consideration of the turbulent properties in the measurement volume indicates that the
 10 three-hour-average estimates of rate of dissipation of turbulent kinetic energy ϵ compares
 11 closely to ~~with the~~ production P_s (Figure 5~~Figure 5a~~). The only departure from this is for a
 12 slack--water low flow period (DOY 300.2-300.6) when the production estimate drops
 13 significantly below the dissipation rate estimate. Under-ice measurements have shown close
 14 correspondence between the dominant turbulence length scale and the inverse of the angular
 15 wavenumber at the peak of the vertical velocity variance spectrum, i.e., $\lambda = c_\lambda / k_{\max}$, where c_λ
 16 is a constant of order unity (McPhee, 2008a; MCPhee and Martinson, 1994). A time series of λ
 17 is compared with the geometric (surface layer) scale $\kappa|z|$ in Figure 5~~Figure 5b~~ which one would
 18 expect to be a limiting scale on the turbulent eddies. The inverse peak wavenumber turbulence
 19 lengthscale sits mostly beneath the geometric scale.

20 When TKE production and dissipation rates are comparable, as suggested by Figure 5a,
 21 the steady, horizontally homogeneous TKE equation provides an independent estimate of
 22 friction speed based exclusively on characteristics of the vertical velocity variance spectrum

$$23 \quad u_* \epsilon = (k_{\max} \epsilon / c_\lambda)^{1/3} u_* = \lambda \epsilon = \frac{c_\lambda}{k_{\max}} \epsilon \quad (4)$$

1 The virtually-independent estimates of friction speed (Figure 5c) agree well. This
2 supports the hypothesis that buoyancy-induced turbulence is minimal in the present conditions.

3 The vertical turbulent heat flux can be estimated from

$$4 \quad H_f = \rho c_p \langle w'T' \rangle \quad (5)$$

5 where ρ is water density and c_p is specific heat of seawater at constant pressure (Figure 6a).
6 Heat flux measurements derived in such a way (Figure 6a) remain entirely
7 negative with the standard deviation being around half the mean value. The heat flux follows
8 a weakly diurnal pattern with broad similarity to u_* (Fig. 5c). The implication then is that a
9 bulk description may be useful as employed for moderate melt rates in water above freezing,
10 so that

$$11 \quad H_f = \rho c_p c_H u_* \Delta T \quad (6)$$

12 where $\Delta T = T - T_f(S, p)$ is the departure from the freezing temperature. The ΔT (Figure 6b),
13 is semidiurnal in structure and so not particularly coupled with the diurnal cycle seen in the
14 calculated and measured heat fluxes (Fig. 6a and c). The departure from the freezing point
15 temperature also exhibits the trend of becoming larger (i.e., increasingly negative) with time during the
16 observation period (Figure 6a,c), and has a negatively increasing trend. Unlike the heat flux
17 estimate, the variability around the mean is reduced. The relationship can be restructured to
18 solve for the transfer coefficient c_H . Averaging the ratio from each of the acceptable 3-hour
19 averages results in $c_H = 0.0085$. Applying this average bulk transfer coefficient and comparing
20 with the measured (Figure 6C) indicates that the bulk approach does reasonable well.
21 Notably, the diurnal cycle, while not apparent in the semidiurnal ΔT , is sufficiently strongly
22 manifest in the u_* .

Formatted: Font: (Default) Times New Roman, Check spelling and grammar

Formatted: Font: (Default) Times New Roman, Check spelling and grammar

Formatted: Font: (Default) Times New Roman

1 **4 Discussion**

2 The questions posed in the introduction relate to how the supercooling and the modified
3 roughness associated with the resulting crystals influence the heat flux. Equation (6) indicates
4 that the problem, for a given temperature difference, can be reduced to a combination of the
5 turbulent heat transfer coefficient c_H and the turbulent velocity scale. The c_H value found here
6 is not far different from values reported for basal heat exchange in above freezing water: e.g.,
7 $c_H = 0.0057$ for the year-long SHEBA project in the western Arctic (McPhee, 2008a); 0.0056
8 for first-year ice in the Weddell Gyre (McPhee et al., 1999). Furthermore, it almost matches
9 the $c_H = 0.0084$ determined for rapid melting in the eastern Arctic (Sirevaag, 2009). This
10 suggests any different behaviour in heat flux is due to the velocity structure induced by the
11 roughness.

12 As identified by Gwyther et al. (2015), the roughness of the boundary affects growth in
13 two ways. First, it influences heat transfer at the ice-ocean interface and second it alters the
14 mixing within, and entrainment into, the basal boundary-layer (BaBL, ~~Figure 1~~Figure 1). While
15 these authors note that sea ice is different to the underside of an ice shelf, it is likely that, at the
16 boundary-layer scale, ~~that~~ the presence of ~~supereool~~ supercooled water and platelets will
17 generate similar effects in the two systems.

18 There is supercooled Ice Shelf Water (ISW) water below the crystals, and these large
19 crystals could not appear from the smaller ISW plume, because such large crystals would be
20 bouyant enough to leave the ISW plume (Jenkins and Bombusch, 1995; Smedsrud and Jenkins
21 2004). They need further heat loss in situ to grow to the large sizes observed, but yet the heat
22 flux through the thick fast ice must be small. The ocean turbulent heat flux was negative
23 (downward) throughout the entire measurement period (Fig. 6a). Sea ice in this region
24 typically forms as congelation ice early in the growth season, then incorporates platelet ice

- Formatted: Font: (Default) Times New Roman, 12 pt
- Formatted: Font: (Default) Times New Roman, 12 pt
- Formatted: Font: (Default) Times New Roman, 12 pt
- Formatted: Font: (Default) Times New Roman, 12 pt
- Formatted: Font: (Default) Times New Roman, 12 pt
- Formatted: Font: (Default) Times New Roman, 12 pt
- Formatted: Font: (Default) Times New Roman, 12 pt

1 towards the end of the growth season (e.g., Smith et al., 2001). Congelation ice grows when the
2 latent heat released during phase change is conducted from the relatively warm ocean to the
3 relatively cold atmosphere. In this context, relatively cold means below the freezing point
4 temperature of seawater. Platelet ice formation occurs in supercooled seawater and when this
5 occurs near the ice/ocean boundary, the latent heat released can either be conducted upwards
6 through the main ice column or transported downwards by turbulent heat flux into the ocean
7 boundary layer. The latter process of negative oceanic heat flux does not occur for congelation
8 ice because the ocean in that case is warmer than the freezing point temperature at the ice-ocean
9 boundary. The ocean turbulent heat flux was negative (downward) throughout the entire
10 measurement period (Figure 6a). Sea ice typically grows in water near or slightly above
11 freezing, where latent heat released during phase change is balanced by upward conduction
12 driven by air temperatures lower than the freezing temperature of seawater. In the absence of
13 horizontal advection, congelation growth in water at freezing temperature requires a small
14 upward ocean heat flux to compensate for salt release. In contrast, platelet nucleation near the
15 ice/ocean boundary releases heat that must be conducted either upward in the main ice column
16 (perhaps against the temperature gradient within the platelet layer, PL Figure 1) or downward
17 by turbulent heat flux in the ocean boundary layer.

18 There is a growing awareness of the ubiquity of such downward heat flux conditions in
19 the vicinity of ice shelves (Robinson et al. 2014; Craven et al., 2015; Hoppmann et al., 2015).
20 The resistance then imposed by a stationary ice cover influenced by such crystal growth on
21 underlying boundary-layer flow depends on the undersurface *hydraulic roughness*, z_0 . For the
22 conditions found at EGT (i.e. $P_s \approx \varepsilon$, undeformed, relatively uniform underice surface), we
23 expect the flow 1 m below the interface to follow the dimensionless shear equation

$$\frac{\kappa |z|}{u_*} \frac{\partial u}{\partial z} = 1 \quad (7)$$

1 where U is mean current speed. The integral of (7) yields a logarithmic velocity profile (the
2 “law of the wall”) where the integration constant is $\log z_0 = -\kappa U / u_*$. For slow currents, the
3 law of the wall is not necessarily valid at 1 m (McPhee, 2008b), so we evaluated $\log z_0$ for 3-
4 hour averages with current speeds $\geq 0.05 \text{ m s}^{-1}$. ~~For U measured at 1 m (i.e. $\log 1 = 0$) the~~
5 average with standard deviation of the acceptable 3-hour samples was

$$\langle \log(z_0) \rangle = -3.95 \pm 0.30 \quad (8)$$

7 The expected value for z_0 is thus about 19 mm.

8 The observed z_0 identified here is larger than values obtained previously from
9 measurements under undeformed fast ice without platelet accumulation, typically found to be
10 nearly hydraulically smooth, with $z_0 \sim 10^{-5} \text{ m}$ (Crawford et al., 1999; MCPhee et al., 2008;
11 MCPhee et al., 2013). It is comparable to values inferred for drifting, multiyear pack ice in the
12 Arctic and western Weddell Sea: $\sim 40 \text{ mm}$ (McPhee, 2008b; Shaw et al., 2009) and is
13 considerably larger than first-year, drifting ice near the center of the Weddell Gyre, $\sim 1 \text{ mm}$
14 (McPhee et al., 1999).

16 5 Conclusions

17 ~~Our data show that we postulate that this~~ turbulence-enhanced transfer of ~~supercool~~
18 ~~supercooled~~ seawater ~~is can be~~ the source of the negative heat flux measured within the ocean
19 boundary layer during the present observations. Our results thus complement the negative
20 ocean heat flux inferred from ice measurements by, e.g., Smith et al. (2012). ~~In addition, Purdie~~
21 ~~et al. (2006) and Gough et al. (2012) estimated of the amount of ice growth through negative~~
22 ~~oceanic heat flux (Figure 7) as additional support for the contention.~~ Furthermore, the
23 downward ocean heat flux, which this work suggests depends on the product of friction speed

Formatted: Font: (Default) Times New Roman, 12 pt, Italic

Formatted: Font: (Default) Times New Roman, 12 pt

Formatted: Font: (Default) Times New Roman, 12 pt

Formatted: Font: (Default) Times New Roman, 12 pt, Font color: Auto

Formatted: Font: (Default) Times New Roman, 12 pt, Font color: Auto

Formatted: Font: (Default) Times New Roman, 12 pt, Font color: Auto

Formatted: Font color: Auto

1 and ΔT , imposes a strong constraint on the rate of ice growth under stationary ice in ~~supercool~~
2 supercooled water. This has significant implications for parametrization of basal boundary-
3 layers beneath both ice shelves and sea ice (Gwyther et al 2015).

4 It is instructive to consider the heat flux distribution as a function of the u^* and ΔT
5 drivers (~~Figure 7~~Figure 7) as there is growing evidence that the presence of ice shelves produces
6 values for both that are outside present expectations. The heat flux contours enable
7 contextualisation of existing results obtained either as measurements of u^* and ΔT pairs or as a
8 heat flux for a particular temperature condition. Parameterisation in terms of u^* suggests
9 timescale is important. While heat flux is typically considered over daily, or longer, timescales
10 so as to compare with seasonal ice growth, u^* will be modulated primarily by tides as direct
11 wind forcing is effectively absent in the present fast ice situation. This is especially important
12 if there is some non-linearity in the growth of more ice as the form of platelets influences u^* .

13 While the present short period of data saw around a factor of 6 variability in H_f (Figure
14 6~~Figure 6~~c) as the two drivers are largely de-coupled, the contours (Figure 7) suggest show that,
15 depending on the local turbulence conditions and degree of supercooling, this variability might
16 approaches two orders of magnitude. Extending this idea, Gwyther et al. (2015) presents a
17 sensitivity analysis that suggest that the variability in u^* through platelet modification of C_d
18 might be as much as an order of magnitude. Future work to address this issue -needs to enhance
19 our focus on understanding of quantifying the combined influence of turbulence, thermally-
20 induced roughness and heat transfer.

21 **Acknowledgements**

23 The authors wish to thank Pat Langhorne for discussion and support. Tim Haskell, Brett Grant,
24 Tim Stanton, Jim Stockel, Alex Forrest, Martin Doble and the staff of Scott Base are thanked

1 for their support in the field. Metadata are lodged with Antarctica New Zealand. Two
2 anonymous reviewers provided helpful comments. The work was funded by The New Zealand
3 Royal Society administered Marsden Fund, and USA NSF support to McPhee (ANT-0732804).
4 Logistic support was provided by Antarctica New Zealand and the USAP.

1 **References**

- 2 Craven, M., Carsey, F., Behar, A., Matthews, J., Brand, R., Elcheikh, A., Hall, S., and
3 Treverrow, A.: Borehole imagery of meteoric and marine ice layers in the Amery Ice Shelf,
4 East Antarctica. *J. Glaciol.*, 51, 75 - 84, doi:10.3189/172756505781829511, 2005.
- 5 Craven, M., Warner, R. C., Galton-Fenzi, B. K., Herraiz-Borreguero, L., Vogel, S. W., and
6 Allison, I.: Platelet ice attachment to instrument strings beneath the Amery Ice Shelf, East
7 Antarctica. *J. Glaciol.*, 60, 383-393, doi:10.3189/2014JoG13J082, 2014.
- 8 Crawford, G., Padman L., and McPhee, M. G.: Turbulent mixing in Barrow Strait, *Cont. Shelf*
9 *Res.*, 19, 205-245. doi:10.1016/S0278-4343(98)00086-7, 1999.
- 10 Crocker, G. B., and Wadhams P.: Modelling Antarctic fast-ice growth, *J. Glaciol.*, 35, 3-8,
11 1989.
- 12 Dayton, P. K., Robilliard G. A., and DeVries A. L.: Anchor ice formation in McMurdo Sound,
13 Antarctica, and its biological effects, *Science*, 163, 274-276, 1969.
- 14 Dempsey, D. E., Langhorne, P. J., Robinson, N. J., Williams, M. J. M., Haskell, T. G., and
15 Frew, R. D.: Observation and modeling of platelet ice fabric in McMurdo Sound,
16 Antarctica, *J. Geophys. Res.: Oceans*, 115(C1), doi:10.1029/2008JC005264, C01007, 2010.
- 17 [Dieckmann, G., Rohardt, G., Hellmer, H. and Kipfstuhl, J.: The occurrence of ice platelets at](#)
18 [250 m depth near the Filchner Ice Shelf and its significance for sea ice biology, *Deep Sea*](#)
19 [Res., Part A, 33, 141–148, 1986.](#)
- 20 Engelhardt, H., and Determann, J.: Borehole evidence for a thick layer of basal ice in the
21 central Ronne Ice Shelf, *Nature*, 327(28), 318–319, 1987.
- 22 Fer, I., Makinson, K., and Nicholls, K., Observations of thermohaline convection adjacent to
23 Brunt Ice Shelf. *J. Phys. Oceanogr.*, 42, 502-508. doi: 10.1175/JPO-D-11-0211.1, 2012.

Formatted: reference, Adjust space between Latin and Asian text, Adjust space between Asian text and numbers

1 Foldvik, A., and Kvinge, T.: Conditional instability of sea water at the freezing point, Deep-
2 Sea Res. 21, 169–174 (doi:10.1016/0011-7471(74)90056-4), 1974.

3 Gough, A. J., Mahoney, A. R., Langhorne, P. J., Williams, M. J. M., Robinson, N. J., and
4 Haskell, T. G.: Signatures of supercooling: McMurdo Sound platelet ice, *J. Glaciol.*, 58, 38-
5 50. doi: 10.3189/2012JoG10J218, 2012.

6 Gow, A. J., Ackley, S., and Govoni, J.W. : Physical and structural properties of land-fast sea
7 ice in McMurdo Sound, Antarctica, *Antarctic Research Series*, 74, 355-374, 1998.

8 Gwyther, D. E., Galton-Fenzi, B. K., Dinniman, M. S., Roberts, J. L., and Hunter, J. R.: The
9 effect of basal friction on melting and freezing in ice shelf ocean models. to appear in *Ocean*
10 *Modelling*, 2015.

11 Hodgson, T. V.: On collecting in Antarctic seas Volume III Zoology and Botany, British
12 National Antarctic Expedition, 1901–1904, Trustees of the British Museum, London, UK, 3,
13 1–10, 1907.

14 Holland, P. R., Corr, H. F. J., Vaughan, D. G., Jenkins, A., and Skvarca, P., Marine ice in
15 Larsen Ice Shelf. *Geophys. Res. Lett.*, 36, L11,604, doi:10.1029/2009GL038162, 2009.

16 Hoppmann, M., Nicolaus, M., Paul, S., Hunkeler, P. A., Heinemann, G., Willmes, S., ... &
17 Gerdes, R. Ice platelets below Weddell Sea landfast sea ice. *Annals of Glaciology*, 56, 175-
18 190, 2015.

19 Hughes, K. G., Langhorne, P. J., Leonard, G. H., and Stevens, C. L. : Extension of an Ice
20 Shelf Water plume model beneath sea ice with application in McMurdo Sound, Antarctica,
21 *J. Geophys. Res.: Oceans*, 119(12), 8662-8687. doi: 10.1002/2013JC009411, 2014.

22 Jeffries, M. O., Weeks, W. F., Shaw, R., and Morris, K.: Structural characteristics of
23 congelation and platelet ice and their role in the development of Antarctic land-fast sea ice,

1 J. Glaciol., 39, 223-238, 1993.

2 [Jenkins, A., and Bombosch A., Modeling the effects of frazil ice crystals on the dynamics and](#)
3 [thermodynamics of the ice shelf water plumes, J. Geophys. Res., 100, 6967–6981, 1995.](#)

4 Kipfstuhl, J., Dieckmann, G., Oerter, H., Hellmer, H., and Graf, W.: The origin of green
5 icebergs in Antarctica, J. Geophys. Res., 97(C12), 20319–20324, 1992.

6 Langhorne, P.: Interactions between ocean, ice shelf, and sea ice. In Proceedings of the 19th
7 International Association of Hydraulic Engineering and Research Symposium on Ice. IAHR
8 & AIRH, Vancouver, Canada, 765-776, 2008.

9 [Langhorne, P.J., Hughes, K.G., Gough, A.J., Smith, I.J., Williams, M.J.M., Robinson, N.J.,](#)
10 [Stevens, C.L., Rack, W., Price, D., Leonard, G.H. and Mahoney, A.R.: Observed platelet ice](#)
11 [distributions in Antarctic sea ice: An index for ocean-ice shelf heat flux. Geophysical](#)
12 [Research Letters, 42\(13\), pp.5442-5451. 2015.](#)

13 Leonard, G. H., Purdie, C. R., Langhorne, P. J., Haskell, T. G., Williams, M. J. M., and Frew,
14 R. D.: Observations of platelet ice growth and oceanographic conditions during the winter
15 of 2003 in McMurdo Sound, Antarctica, J. Geophys. Res.: Oceans, 111(C4), C04012,
16 doi:10.1029/2005JC002952, 2006.

17 Leonard, G. H., Langhorne, P. J., Williams, M. J. M., Vennell, R., Purdie, C.R., Dempsey, D.
18 E., Haskell, T. G., and Frew, R. D.: Evolution of supercooling under coastal Antarctic sea
19 ice during winter, Antarctic Science, 23, 399-409, doi:10.1017/S0954102011000265, 2011.

20 Lewis, E. L., and Perkin, R.G. : The winter oceanography of McMurdo Sound, Antarctica,
21 Antarctic Research Series, 43, 145-165, 1985.

22 Lewis, E. L., and Perkin, R. G.: Ice pumps and their rates, J. Geophys. Res., 91(C10), 11756-
23 11762, 1986.

Formatted: reference, Adjust space between Latin and Asian text, Adjust space between Asian text and numbers

1 Mahoney, A. R., Gough, A. J., Langhorne, P. J., Robinson, N. J., Stevens, C. L., Williams,
2 M. J. M., and Haskell, T. G.: The seasonal appearance of ice shelf water in coastal
3 Antarctica and its effect on sea ice growth, *J. Geophys. Res.: Oceans*, 116(C11), C11032.
4 doi:10.1029/2011JC007060, 2011.

5 McPhee, M. G.: On the Turbulent Mixing Length in the Oceanic Boundary Layer, *J. Phys.*
6 *Oceanog.*, 24, 2014-2031, 1994.

7 McPhee, M. G.: Air-Ice-Ocean Interaction: Turbulent ocean boundary layer exchange
8 processes, ix, 215 p. pp., Springer, New York, 2008a.

9 McPhee, M. G. : Physics of early summer ice/ocean exchanges in the western Weddell Sea
10 during ISPOL, *Deep Sea Research Part II: Topical Studies in Oceanography*, 55, 1075-1097,
11 2008b.

12 McPhee, M. G., and Martinson, D. G.: Turbulent Mixing Under Drifting Pack Ice in the
13 Weddell Sea, *Science*, 263(5144), 218-221, 1994.

14 McPhee, M. G., Kottmeier, C., and Morison, J. H.: Ocean Heat Flux in the Central Weddell
15 Sea during Winter, *J. Phys. Oceanog.*, 29, 1166-1179, 1999.

16 McPhee, M. G., Morison, J. H., and Nilsen, F.: Revisiting heat and salt exchange at the ice-
17 ocean interface: Ocean flux and modeling considerations, *J. Geophys. Res.: Oceans*,
18 113(C6), C06014, 2008.

19 McPhee, M. G., Skogseth, R., Nilsen, F., and Smedsrud, L.H.: Creation and tidal advection of
20 a cold salinity front in Storfjorden: 2. Supercooling induced by turbulent mixing of cold
21 water, *J. Geophys. Res.: Oceans*, 118, 3737-3751. doi:10.1002/jgrc.20261, 2013.

22 Paige, R. A.: Crystallographic studies of sea ice in McMurdo Sound, *AntarcticaRep.*, 31 pp,
23 US Naval Civil Engineering Laboratory, Port Hueneme, California, USA, 1966.

- 1 Purdie, C. R., Langhorne, P. J., Leonard, G. H., and Haskell, T. G. : Growth of first-year
2 landfast Antarctic sea ice determined from winter temperature measurements, *Annals of*
3 *Glaciology*, 44, 170-176, 2006.
- 4 Robin, G. d. Q., Doake, C. S. M., Kohnen, H., Crabtree, R. D., Jordan, S. R., and Möller, D.:
5 Regime of the Filchner-Ronne ice shelves, *Antarctica, Nature*, 302(14), 582–586, 1983.
- 6 Robinson, N. J., Williams, M. J. M., Stevens, C. L., Langhorne, P. J., and Haskell, T. G.:
7 Evolution of a supercooled Ice Shelf Water plume with an actively growing subice platelet
8 matrix, *J. Geophys. Res.: Oceans*, 119(6), 3425-3446. doi:10.1002/2013JC009399, 2014.
- 9 Shaw, W. J., Stanton, T. P., McPhee, M. G., Morison, J. H., and Martinson, D. G.: Role of the
10 upper ocean in the energy budget of Arctic sea ice during SHEBA, *J. Geophys. Res.:*
11 *Oceans*, 114(C6), C06012, 2009.
- 12 Sirevaag, A.: Turbulent exchange coefficients for the ice/ocean interface in case of rapid
13 melting, *Geophys. Res. Lett.*, 36(4), L04606, 2009.
- 14 Sirevaag, A., McPhee, M. G., Morison, J. H., Shaw, W. J., and Stanton, T. P.: Wintertime
15 mixed layer measurements at Maud Rise, Weddell Sea, *J. Geophys. Res.: Oceans*, 115(C2),
16 C02009. doi: 10.1029/2008JC005141, 2010.
- 17 [Smedsrud, L. H., and Jenkins, A., Frazil ice formation in an ice shelf water plume, J.](#)
18 [Geophys. Res., 109, C03025, doi:10.1029/2003JC001851, 2004.](#)
- 19 Smith, I. J., Langhorne, P. J., Frew, R. D., Vennell, R., and Haskell, T. G.: Sea ice growth
20 rates near ice shelves, *Cold Regions Science and Technology*, 83–84, 57-70, 2012.
- 21 Smith, I. J., Langhorne, P. J., Todahl, H. J., Haskell, T. G., Frew, R., and Vennell, R.:
22 Platelets ice and the land-fast sea ice of McMurdo Sound, *Antarctica, Annals of Glaciology*,
23 33, 21-27, 2001.

Formatted: reference, Adjust space between Latin and Asian text, Adjust space between Asian text and numbers

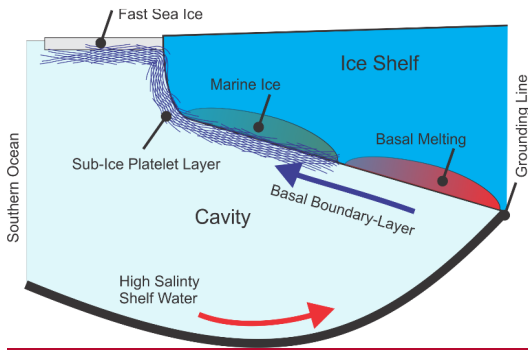
- 1 Smith, I. J., Gough, A. J., Langhorne, P. J., Mahoney, A. R., Leonard, G. H., van Hale, R.,
2 Jendersie, S., and Haskell, T. G.: First-year land-fast Antarctic sea ice as an archive of ice
3 shelf meltwater fluxes. *Cold Regions Science and Technology* 113, 63-70, 2015.
- 4 Stevens, C. L., Robinson, N. J., Williams, M. J. M., and Haskell, T. G.: Observations of
5 turbulence beneath sea ice in southern McMurdo Sound, Antarctica, *Ocean Science*, 5, 435-
6 445. doi:10.5194/os-5-435-2009, 2009.
- 7 Stevens, C. L., McPhee, M. G., Forrest, A. L., Leonard, G. H., Stanton, T., and Haskell, T. G.:
8 The influence of an Antarctic glacier tongue on near-field ocean circulation and mixing, *J.*
9 *Geophys. Res.: Oceans*, 119(4), 2344-2362, doi:10.1002/2013JC009070. 2014.
- 10 Tennekes, H., Lumley, J.L. A first course in turbulence. MIT press, 1972.
- 11 Wright, C. S., and Priestley, R. E.: *Glaciology – British (Terra Nova) Antarctic Expedition,*
12 1910–1913, Harrison and Sons, London, U.K., 1922.

13
14

Formatted: reference

1 **Figures**

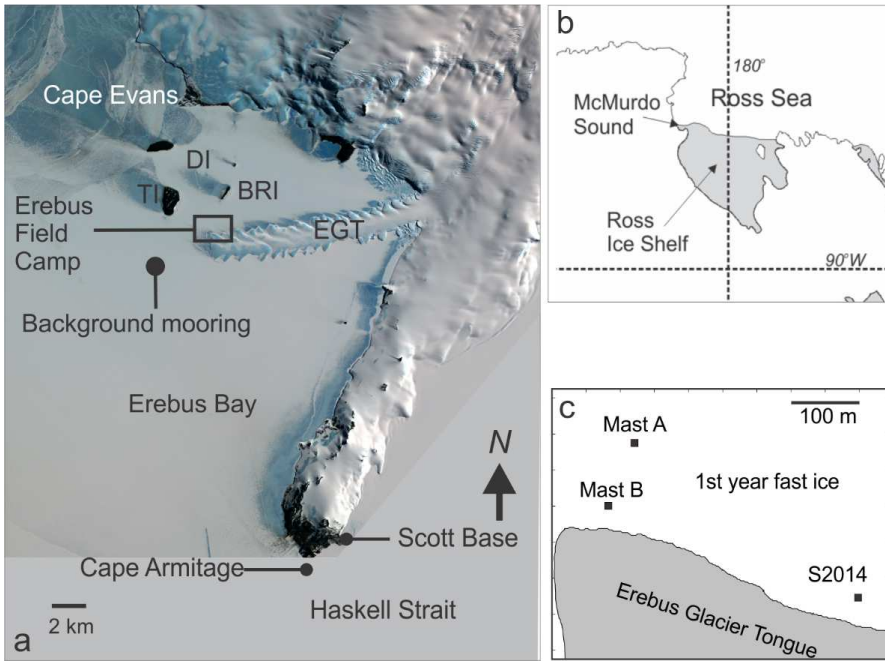
2
3



4

Figure 1 Ice pump showing high salinity shelf water (HSSW) flowing in at the base of an ice shelf cavity, commencing basal melting (BM) at, or around, the grounding line (GL). This buoyant meltwater flows upwards and outwards in a basal boundary-layer (BaBL). An associated platelet-forming layer (PL) supports ice growth through freezing into marine ice (MI) and PL beneath fast sea ice.

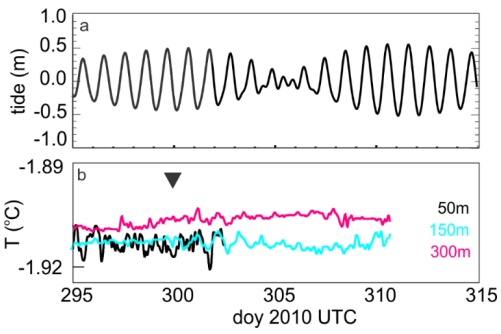
5



1

Figure 2 (a) McMurdo Sound, Antarctica, in the context of the Ross Ice Shelf and the Ross Sea. (b) SW McMurdo Sound image from ASTER (Advanced Space borne Thermal Emission and Reflection Radiometer) satellite image of south east McMurdo Sound including the Erebus glacier tongue (EGT), the Dellbridge Islands (DI), Erebus Bay (EB), Cape Evans (CE), Cape Armitage (CA), Haskell Strait (HS), Scott Base (SB), background mooring (BG) and the Erebus field camp (EFC). The Dellbridge Islands include Tent Island (TI) and Big Razorback Island (BRI). (b) The McMurdo Sound region, Antarctica, in the context of the Ross Ice Shelf and the Ross Sea. (c) Erebus Field Camp locale showing the turbulence mast locations relative to the edge of EGT.

2



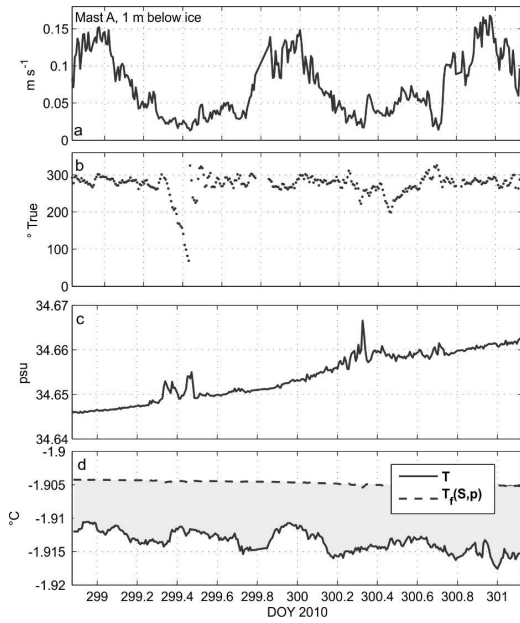
1

Figure 3 (a) tidal elevation and (b) in situ temperatures from background mooring (BG in [Figure 2](#)). The time of the present detailed observations are marked with the triangle in (b). The sensor at 50 m stopped early due to battery exhaustion.

2

3

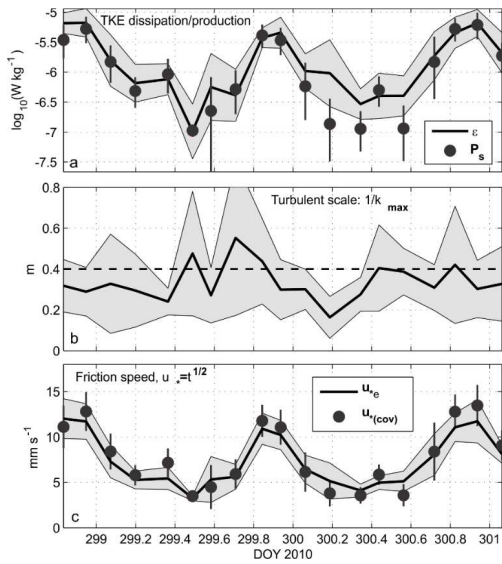
1



2

Figure 4 (a) Current speed at 1 m below the ice/ocean boundary from Mast A. (b) Current direction (bearing from true north). (c) Salinity (practical salinity scale). (d) Water temperature (solid) and water freezing temperature at 2 m depth (dashed).

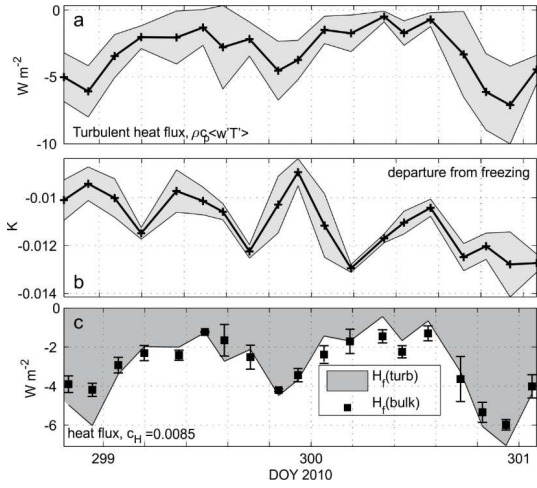
3



1

Figure 5 (a) Three-hour averages of turbulent kinetic energy dissipation rate (solid with shading showing ± 1 std. deviation of the 15-min realizations in each average) and TKE production by shear (circles with std. deviation). (b) Turbulent length scale from the inverse wavenumber at w variance spectral peaks. Dashed line indicates the “geometric” surface layer scale, $\kappa|z|$. (c) Independent estimates from of friction speed from w variance spectra (solid with shading) and from covariance statistics (circles with std. deviation bars).

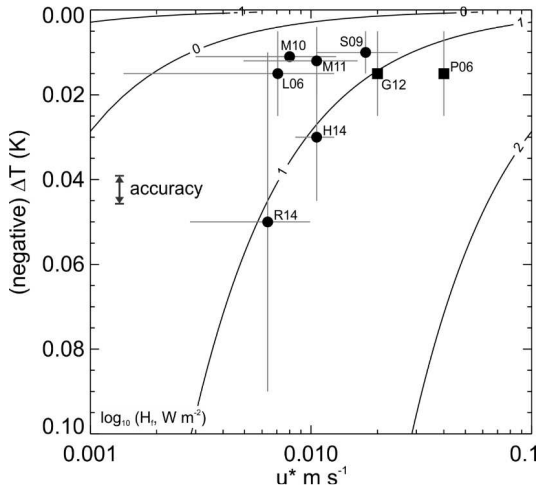
1



2

Figure 6 (a) Three-hour averages of turbulent heat flux, solid with std. deviation shading. (b) Departure of temperature from in situ freezing point temperature. (c) Comparison showing measured heat flux (shaded) with bulk estimates based on the product of u_s and ΔT using the transfer coefficient identified using equation (6).

3



1
2
3 Figure 7 Contours of \log_{10} of heat flux H_f , as a function of friction speed u^* and thermal
4 driving ΔT , for present c_H estimate. Contours describe equation (6). Circles are from
5 measurements of u^* and ΔT , (L06 Leonard et al 2006; S09 Stevens et al. 2009; M11 Mahoney
6 et al. 2011; H14 Hughes et al. 2014; R14 Robinson et al. 2014 and M10 this study). The
7 “error-bars” represent degree of variability. The u^* were either directly measured (i.e. M10)
8 or inferred from flow U using a drag coefficient whereby $u^*=(C_d)^{1/2}U$. The squares are from
9 observations inferring heat flux so that a u^* is inferred given the observed ΔT (P06 Purdie et
10 al. 2006; G12 Gough et al. 2012).